Development 137, 4155-4164 (2010) doi:10.1242/dev.034355

N-cadherin acts in concert with Slit1-Robo2 signaling in regulating aggregation of placode-derived cranial sensory neurons

Celia E. Shiau and Marianne Bronner-Fraser*

Vertebrate cranial sensory ganglia have a dual origin from the neural crest and ectodermal placodes. In the largest of these, the trigeminal ganglion, Slit1-Robo2 signaling is essential for proper ganglion assembly. Here, we demonstrate a crucial role for the cell adhesion molecule N-cadherin and its interaction with Slit1-Robo2 during gangliogenesis in vivo. A common feature of chick trigeminal and epibranchial ganglia is the expression of N-cadherin and Robo2 on placodal neurons and Slit1 on neural crest cells. Interestingly, N-cadherin localizes to intercellular adherens junctions between placodal neurons during ganglion assembly. Depletion of N-cadherin causes loss of proper ganglion coalescence, similar to that observed after loss of Robo2, suggesting that the two pathways might intersect. Consistent with this possibility, blocking or augmenting Slit-Robo signaling modulates N-cadherin protein expression on the placodal cell surface concomitant with alteration in placodal adhesion. Lack of an apparent change in total N-cadherin mRNA or protein levels suggests post-translational regulation. Co-expression of N-cadherin with dominant-negative Robo abrogates the Robo2 loss-of-function phenotype of dispersed ganglia, whereas loss of N-cadherin reverses the aberrant aggregation induced by increased Slit-Robo expression. Our study suggests a novel mechanism whereby N-cadherin acts in concert with Slit-Robo signaling in mediating the placodal cell adhesion required for proper gangliogenesis.

KEY WORDS: Cadherins, Slits/Robos, Placode, Neural crest, Gangliogenesis, Trigeminal, Chick

INTRODUCTION

During development, proper formation of various organs and structures requires coordinated interactions between different cell types. In vertebrates, a prime example is the interaction between neural crest and ectodermal placodes, two cell types of distinct embryonic origin, both of which contribute to the ganglia of the head (D'Amico-Martel and Noden, 1983). The cranial sensory ganglia – trigeminal, geniculate (facial), petrosal (glossopharyngeal) and nodose (vagal) – are essential components of the peripheral nervous system that relay sensory information, such as pain, touch and temperature, from the head and various organs to the brain (Baker, 2005). These ganglia form adjacent and external to the forming midbrain and hindbrain and make central connections to even-numbered rhombomeres (Noden, 1993). Formation of the cranial sensory ganglia requires cell-cell communication that facilitates intermixing, proper positioning and aggregation of placode and neural crest cells into discrete ganglionic structures. However, the signals and effector molecules that coordinate their proper condensation into the cranial ganglia are largely uncharacterized.

Neural crest cells play a crucial role in organizing placodal neurons during early ganglion assembly. The position and shape of the cranial ganglia largely mirror the migration patterns of the cranial neural crest. Moreover, ablation of the dorsal midbrain neural folds causes abnormalities in trigeminal ganglion assembly, demonstrating that neural crest cells are required for the proper organization and integration of placodal neurons into the ganglion (Shiau et al., 2008). Loss of the receptor neuropilin 2, which is expressed by neural crest cells, and/or of semaphorin ligands, which are expressed in the adjacent mesenchyme, causes defects in neural crest migration that lead to malpositioning of neuronal cell bodies and axons. This results in aberrantly interlinked trigeminal and facial ganglia (Gammill et al., 2006; Schwarz et al., 2008). Cell-cell signaling between neural crest and placodes is likely to mediate their coordinated and cooperative interactions in forming the cranial ganglia. For example, trigeminal placode cells express Robo2, whereas neural crest cells express its cognate ligand Slit1. Blocking either receptor or ligand function causes severe malformations, such as aberrantly or diffusely condensed ganglia (Shiau et al., 2008).

Slit signaling through Robo receptors in the central nervous system midline plays a broadly conserved role in axon repulsion in both invertebrates and vertebrates (Brose and Tessier-Lavigne, 2000; Dickson and Gilestro, 2006). In addition, Slits and Robos have been implicated in heart tube morphogenesis in the fruit fly, in which they appear to regulate cell adhesion and cell polarity genes (MacMullin and Jacobs, 2006; Qian et al., 2005; Santiago-Martinez et al., 2006), including *E-cadherin* (*shotgun* – FlyBase) (Santiago-Martinez et al., 2008). In chick neural retinal cultures, as well as in mouse fibroblast L-cells that express N-cadherin (cadherin 2 – Mouse Genome Informatics), Slit activation of Robo appears to inhibit N-cadherin function (Rhee et al., 2002). The cell biological effects downstream of Slit-Robo signaling during vertebrate development remain elusive.

Because cell-cell interactions appear important for trigeminal ganglion formation, we examined the role of the cell-cell adhesion molecule N-cadherin in ganglion assembly and tested for possible links between N-cadherin-mediated adhesion and Slit-Robo signaling. N-cadherin is a member of the type I classical cadherins (as are the E- and R-cadherins). These are transmembrane, Ca^{2+}-dependent adhesion molecules that preferentially bind

Division of Biology 139-74, California Institute of Technology, Pasadena, CA 91125, USA.

*Author of correspondence (mbronner@caltech.edu)

Accepted 12 October 2009

homophilically through their extracellular domains (Gumbiner, 2005). In vertebrates, N-cadherin is expressed in neural crest-derived spinal ganglia (Akitaya and Bronner-Fraser, 1992; Inuzuka et al., 1991; Packer et al., 1997; Redies et al., 1992) and has been implicated in shaping the sympathetic chain ganglia (Kasemeier-Kulesa et al., 2006). N-cadherin is also expressed in chick sensory fibers at stages 29-37 (E6-E11) (Redies et al., 1992) and in mouse E12.5 cranial nerves (Packer et al., 1997). However, little is known about its early expression or function during cranial ganglia assembly in amniotes. In zebrafish, N-cadherin appears to be important for cranial ganglia formation (Kerstetter et al., 2004; Liu et al., 2003), although it is not yet clear whether it functions in neural crest cells, placodes, or both.

Here, we show in chick that N-cadherin is expressed by placode-derived sensory neurons and is required for ganglion condensation. Our data suggest that N-cadherin acts cooperatively with Slit1-Robo2 signaling during gangliogenesis in mediating the aggregation of placode-derived sensory neurons into cranial ganglia.

MATERIALS AND METHODS

Embryos

Fertilized chicken (*Gallus gallus domesticus*) eggs were obtained from local commercial sources and incubated at 37°C to the desired stages.

In situ hybridization

Whole-mount chick in situ hybridization was performed as described (Shiau et al., 2008). cDNA templates used for antisense riboprobes were chick *Slit1* and *Robo2* as described (Vargesson et al., 2001). Embryos were imaged and sectioned at 12 μm.

Immunohistochemistry

Primary antibodies used were anti-N-cadherin (DSHB, MNCD2 clone, 1:1; and Abcam, clone 12221, 1:250), anti-GFP (Molecular Probes, 1:1000-1:2500), anti-HNK-1 (American Type Culture Collection, 1:3-1:5), anti-Islet1 (DSHB, clone 40.2D6, 1:250), anti-TuJ1 (Covance, 1:250) and anti-β-catenin (Sigma, clone 15B8, 1:300). Secondary antibodies were cyanine 2 or rhodamine red-x conjugated donkey anti-rat IgG (Jackson ImmunoResearch, 1:250) and all other secondary antibodies were obtained from Molecular Probes. Images were taken on a Zeiss Axioskop2 Plus or DeltaVision Spectris fluorescence microscope and processed using Adobe Photoshop CS3.

In ovo electroporation of the trigeminal ectoderm

All constructs were introduced prior to ingression at stages 8-10 to transfect both the placodal ectoderm and derived cells in the ganglionic anlage. Platinum electrodes were placed vertically across the chick embryo delivering five current pulses of 8 V in 50 milliseconds at 100-millisecond intervals as described (Shiau et al., 2008). Incubation was then continued for ~18-24 hours to reach stages 13-14, ~28-36 hours to reach stages 15-16, or ~40-48 hours to reach stages 17-18.

Plasmid constructs and morpholinos

DNA plasmids used were Robo2Δ-GFP (Hammond et al., 2005), FL-Robo2 (CMV-Robo2FL-myc) (Reeber et al., 2008) and, for control GFP expression, cytoplasmic GFP (cytopcig) (Shiau et al., 2008) and membrane GFP (pCAβ-IRES-mGFP) (McLarren et al., 2003). For constructing the cytopcig-Slit1-LRR vector, full-length chick *Slit1* cDNA was isolated from a 4- to 12-somite chick macroarray library as described (Gammill and Bronner-Fraser, 2002), which contains the coding sequence for the first 863 amino acids of chick Slit1 with a 3× FLAG tag. For creating the cytopcig-FL-Ncad vector, a full-length chick N-cadherin fragment (starting 5 bp upstream of ATG) was amplified from the pCMV-cN/FLAG-pA vector (Nakagawa and Takeichi, 1998). The morpholino oligomer (Gene Tools, LLC) against the start site of chick N-cadherin (Ncad MO) was 5′-GCGGCGTTCCCGCTATCCGGCACAT-3′. Standard control oligomer from Gene Tools (control MO) and Ncad MO were both 3′ lissamine or 3′ fluorescein tagged, diluted with water and used at 1 μM.

RNA extraction and quantitative PCR (qPCR)

Total RNA was isolated using the RNAqueous-Micro RNA Isolation Kit (Ambion). qPCR was performed using the ABI Prism 7000 Sequence Detection System (Applied Biosciences) with SYBR Green real-time PCR reagent (Bio-Rad). Reactions (25 μl) comprised 2× SYBR Green mix (Bio-Rad), each primer at 450 nM (except 150 nM for *Gapdh* primers), and ~1.5-1.8 μg of cDNA. For primer sequences, see Fig. S4 in the supplementary material. Gene expression levels were assessed using the comparative C_T (threshold cycle) method as described in the Applied Biosystems manual.

Protein extraction and western blot analysis

Chick embryonic head tissues between the posterior border of the eye and the first branchial arch at rhombomere 1/2 containing the trigeminal ganglia were excised in Ringer's buffer and snap frozen in an ethanol/dry ice bath. Each head tissue was independently collected and homogenized in 100 μl of lysis buffer comprising 50 mM Tris-HCl (pH 8.0), 100 mM NaCl, 5 mM EDTA, 1% Nonidet P40 and Complete Protease Inhibitor (Roche). Semi-quantitative comparisons of N-cadherin protein levels in control and dnRobo2 embryos were made by ImageQuant (Amersham) analysis of SDS-PAGE gels. Primary antibodies used were anti-N-cadherin (Abcam, clone 12221) and anti-α-tubulin (Invitrogen, clone B512). Blots were visualized using ECL Plus western blotting detection reagents (Amersham).

Quantification of placodal dispersion

Dispersion of trigeminal placodal neurons was quantitated using the ImageJ area calculation function to measure the area spread of the trigeminal neurons as marked by TuJ1 staining in whole-mount images of stage 15-16 heads. Grayscale images of ganglia were converted to binary scale and a threshold was set to cover the spread of TuJ1 staining; small gaps were filled in to calculate the area. Areas of the experimental ganglia were normalized to the average control ganglia area.

RESULTS

N-cadherin is expressed by trigeminal and epibranchial placodal neurons but not cranial neural crest during gangliogenesis

To determine whether N-cadherin plays a role in cranial gangliogenesis, we first examined its expression pattern in the developing chick embryo from stages 13-17, as the trigeminal and epibranchial ganglia assemble and aggregate (Fig. 1). Neural crest cells begin to differentiate into neurons late in development after the ganglia are well condensed at stages ~22-24 (D'Amico-Martel and Noden, 1980; D'Amico-Martel and Noden, 1983). Therefore, broad neuronal markers, such as Islet1 and β-neurotubulin (TuJ1), uniquely label placodal cells during early ganglion assembly. Cell-marking techniques, such as GFP electroporation in the ectoderm, can also reliably label the placodal ectoderm and derived neurons.

During initial ganglion formation, N-cadherin expression is restricted to placode but not neural crest cells. Using immunohistochemistry with antibodies to N-cadherin, neural crest marker HNK-1 (a carbohydrate epitope also known as Leu-7), and placodal neuronal marker TuJ1 or Islet1, we observed expression of N-cadherin on TuJ1- and Islet1-positive cells, but not on HNK-1-expressing cells, at all stages, leading to well-condensed ganglia (Fig. 1). N-cadherin staining was apparent both in the placodal ectoderm and in those placodes that had ingressed; expression continued through the time of cranial ganglia assembly (Fig. 1). Consistent with previous reports, we also found high levels of N-cadherin expression in the neural tube, notochord and lens (Hatta et al., 1987; Hatta and Takeichi, 1986) and slightly lower levels in the mesoderm-derived mesenchyme.

Interestingly, N-cadherin levels fluctuated dynamically in placodal tissue as a function of time. In the trigeminal region, most of the surface ectoderm, except that overlying the dorsal neural tube, expressed N-cadherin at times of early ingression at stage 13 (Fig.

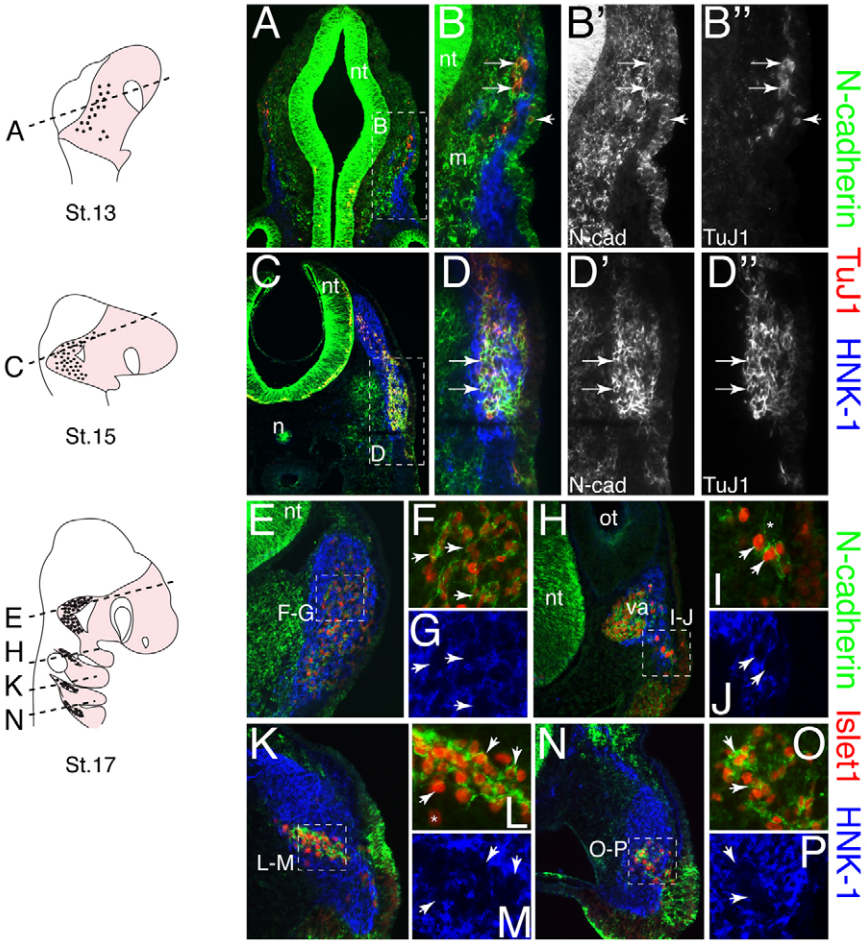

Fig. 1. Expression of chick N-cadherin protein on trigeminal and epibranchial ectodermal and ingressing placode-derived neurons. Schematics on left indicate the levels of the sections (dashed lines), the neural crest region (pink) and placodes (black dots). Placode-derived neurons are marked by β-neurotubulin (TuJ1) or Islet1, and neural crest cells by HNK-1. (**A**) Stage 13 showing ingressing trigeminal placodes. (**B-B″**) Higher magnification of boxed region in A. Ingressed placodal cells (arrows) and ectodermal placodes (arrowhead) co-express TuJ1 and N-cadherin. (**C-D″**) Stage 15 in the early forming trigeminal ganglion. N-cadherin expression overlaps with the placodal marker TuJ1 (arrows), but not with HNK-1, at all stages. (**E-P**) Stage 17 in the condensing (E-G) trigeminal, (H-J) facial (or geniculate), (K-M) glossopharyngeal (or petrosal), and (N-P) vagal (or nodose) ganglionic regions. Few Islet1-negative cells express N-cadherin at stage 17 (I, star). Islet1^{+} cells co-express N-cadherin (arrowheads), with some exceptions of individual placodal cells (L, star). HNK-1^{+} neural crest cells do not express N-cadherin at all cranial axial levels. N-cad, N-cadherin; nt, neural tube; m, mesoderm; n, notochord; ot, otic vesicle; va, vestibuloacoustic ganglion.

1A,B). Later, at stages 15-17, N-cadherin expression was downregulated in the ectoderm (Fig. 1C-E), although expression persisted in the frontonasal ectoderm, including the lens (data not shown). The discrete spots of low-level expression in the ectoderm at later stages may correlate with sites of placodal ingression, which continues through stage 21 (D'Amico-Martel and Noden, 1983). At the tissue level, N-cadherin expression in the ingressed placodal neurons appeared to increase with time, changing from punctate at stage 13 (Fig. 1A,B) to a more continuous membrane expression by stage 15 (Fig. 1C-G), when the ganglion is condensing. We primarily used antibody to Islet1 to identify placodal neurons later, at stage 17, because this nuclear marker can be easily distinguished from N-cadherin, so as to visualize individual placodes with the N-cadherin expression domain. N-cadherin was co-expressed with TuJ1 at stage 17 around the cell bodies, but less prominently in the axonal processes (see Fig. S1 in the supplementary material). Similar to the trigeminal placode, we observed N-cadherin expression in the epibranchial ectoderm and in the ingressing placode cells thereof (Fig. 1H-P).

N-cadherin is essential for proper placodal aggregation and trigeminal ganglion assembly

To test the function of N-cadherin in placodal cells during gangliogenesis, we focused on the forming trigeminal ganglion because of its large size and characteristic semilunar shape, which aids in systematic scoring of phenotypes. To deplete N-cadherin from placodal cells, we used a translation-blocking antisense morpholino oligomer (MO) against chick N-cadherin (Ncad MO). MOs were introduced by in ovo electroporation into the presumptive trigeminal placodal ectoderm at axial levels between the forming forebrain and otic region at stages 8-10 prior to placodal ingression. Ganglionic defects were scored at stages 15-18 as 'mild' or 'severe' in control and experimental embryos (Fig. 2A,B). 'Mild' defects were defined as those displayed by ganglia in which the overall shape was discernible but were misshapen with numerous abnormal protrusions and dispersed individual cells outside of the normal trigeminal area. 'Severe' defects were displayed by ganglia in which trigeminal neurons were widely dispersed and failed to assume the normal bilobed morphology (Fig. 2B). The results showed that depleting N-cadherin in the trigeminal placodal ectoderm and derived neurons leads to significantly dispersed placodal neurons in the forming ganglia at stages 15-16 (29% severe and 42% mild defects, n=24) and to misshapen ganglia at stages 17-18 when the ganglia are well condensed (31% mild defects, n=13) (Fig. 2B,C). Although we cannot rule out the possibility that there is some recovery with time, it seems more likely that the observed reduction in the severity of the phenotype at the later stages is due to dilution of the MO. By contrast, control MO embryos showed little or no effect (Fig. 2A,C) at all time points examined.

To measure the level of dispersion of the trigeminal placode cells caused by N-cadherin depletion, we quantitated the area occupied by TuJ1^{+} placodal neurons in control versus severely affected Ncad MO-treated embryos using the ImageJ area calculation from whole-mount images of the entire trigeminal region at stages 15-16 (Fig. 2C). There was a highly significant difference in the area occupied

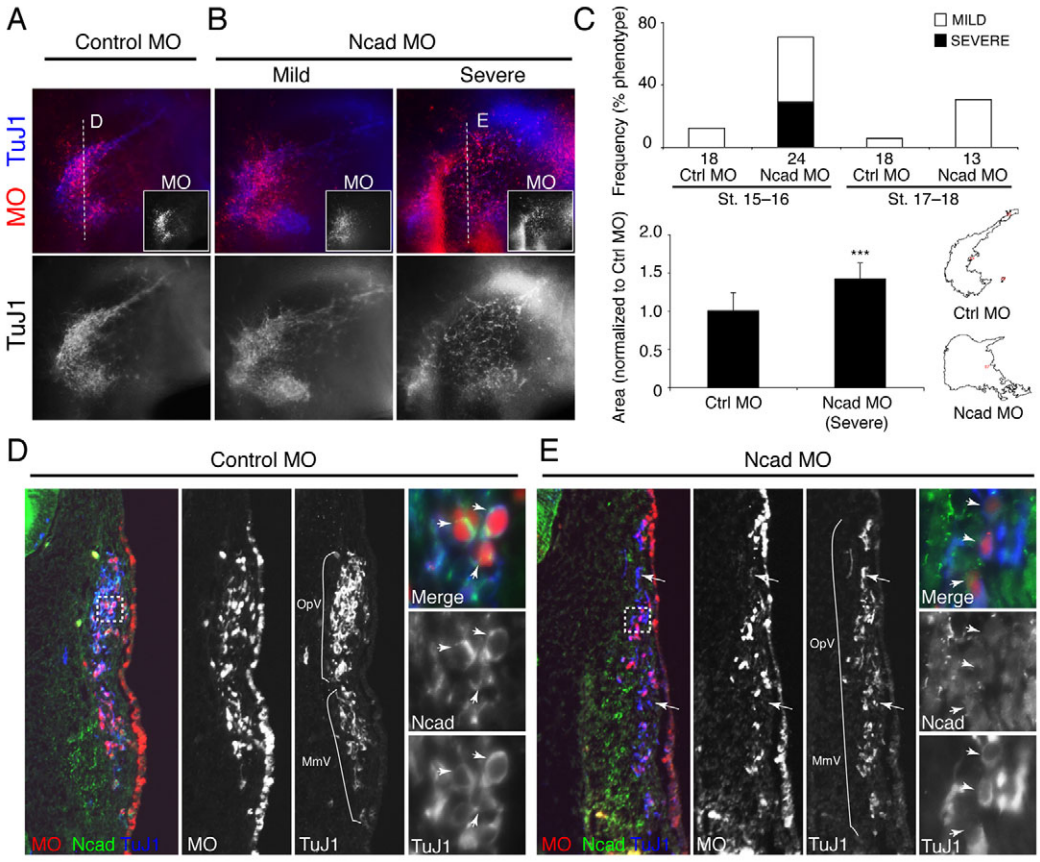

Fig. 2. N-cadherin knockdown blocks proper trigeminal placodal aggregation. (**A**) Control MO trigeminal ganglion. (**B**) Ncad MO showing 'mild' and 'severe' phenotypes at stages 15-16. (**C**) (Above) A high percentage of ganglionic defects in Ncad MO embryos at stages 15-16 and a lower percentage at stages 17-18, with little effect in controls. The number ganglia analyzed (*n*) is shown beneath each bar. (Below) Significantly more dispersed trigeminal placodal ganglia in severely affected Ncad MO embryos (1.42±0.21) relative to controls (1.0±0.24) (***P=0.0003, two-tailed Student's *t*-test) using ImageJ area analysis. Error bars, s.d. To the right are shown representative outlines of calculated placodal areas. (**D**,**E**) Frontal plane sections through the same embryos as in A and B at the level indicated by the dashed lines. Placodal neurons in the Ncad MO ganglion were markedly more scattered. Panels showing MO alone indicate the area of transfection, and those showing TuJ1 alone indicate the distribution of placodes. The boxed region is shown at higher magnification to the right; arrows indicate N-cadherin reduction in Ncad MO but not control MO placodes. (E) A few scattered placode-derived neurons do not have Ncad MO (arrows). OpV and MmV lobes are not distinct in the Ncad MO embryo, as compared with the control (brackets). Ctrl, control; Ncad, N-cadherin; MO, morpholino; OpV, ophthalmic; MmV, maxillomandibular.

by placode-derived neurons of control versus severely affected experimental embryos, with the latter having a greater than 40% increase in ganglion area (P=0.0003). Sections revealed that the bilobed clustering of the ganglia was clearly disrupted in the N-cadherin-depleted placodal cell population (compare Fig. 2D,E). Placodal neurons were markedly more scattered, with concomitant reduction in N-cadherin protein expression (Fig. 2E). The results suggest that loss of N-cadherin in placodal cells reduces cell-cell contact and abrogates clustering of placodal neurons (Fig. 2E), consistent with the dispersed ganglia observed in whole-mount. It should be noted that a few cells that did not contain MO also appeared to be dispersed (Fig. 2E). Such non-cell-autonomous effects are not surprising given that there is a high degree of cell-cell contact between placodal cells, and N-cadherin is normally highly expressed at sites of cell contact. Thus, if the majority of placode cells were electroporated with Ncad MO, the neighboring wild-type cells may lack proper neighbors with which to adhere. However, the effect appears to be specific to the placodal ectoderm rather than a general consequence of lower adhesion in ectoderm tissue, as electroporation of Ncad MO into neighboring ectodermal regions that do not contribute to the trigeminal ganglion had no effect on trigeminal ganglion formation (data not shown). The effectiveness of Ncad MO in depleting N-cadherin protein was confirmed by immunohistochemistry in the lens (see Fig. S2 in the supplementary material), where N-cadherin expression is persistent and strong, and in the trigeminal placode cells (Fig. 2E), both of which showed a marked reduction in protein levels compared with control MO embryos.

The effects of dispersed and disorganized placodal neurons in the forming trigeminal ganglion observed with Ncad MO are reminiscent of the defects caused by Robo2 loss-of-function (Shiau et al., 2008). The co-expression of N-cadherin and Robo2 on ingressed placode-derived neurons, together with the required functions of N-cadherin and Robo2 signaling for proper placodal coalescence, raises the intriguing possibility of a cooperative interaction between the two pathways for ganglion assembly. However, defects in axon guidance were more pronounced in the Robo2-deficient embryos.

N-cadherin plays no obvious role in placodal ingression

Since N-cadherin is expressed dynamically in both surface ectoderm and ingressing placodal cells after detachment, we asked whether N-cadherin is required for the ingression of placodal neurons. We counted the total number of placodal cells, identified by Islet1-positive staining, in 10 μm frontal sections collected from the entire presumptive trigeminal region at times of early and abundant ingression at stage 14 (boxed region in Fig. 3). The number of placodal neurons associated with the surface ectoderm (either in ectoderm or adjacent to its basal margin) versus the mesenchyme was analyzed as previously described (Shiau et al., 2008). These two categories represent the populations of placodal neurons that are initiating ingression and those that have already ingressed, respectively. No significant difference was observed in the percentage of Islet1$^+$ placodal cells that had ingressed in Ncad MO (63.7±3.9%, n=3) versus control MO (67.8±7.6%, n=4) embryos (Fig. 3A). This suggests that reducing N-cadherin levels has little or no effect on placodal cell ingression. However, MO knockdown is never complete, leaving open the possibility that N-cadherin might play an as yet undetected role in this process.

The lack of any significant difference in the percentage of ingressed cells between Ncad MO and control MO embryos (Fig. 3) contrasts with the effect of loss of Robo2, which causes a greater than 2-fold decrease in ingression (Shiau et al., 2008). This suggests that the Robo2-dependent ingression process does not rely on N-cadherin. However, placodal cells in Ncad MO-treated embryos appeared more dissociated, even at early stages of ingression (compare Fig. 3B,C). Thus, N-cadherin might be one of several downstream mediators or interacting partners of Slit-Robo signaling that act in concert to mediate proper placodal gangliogenesis.

Perturbation of Slit1-Robo2 signaling can alter N-cadherin protein expression in vivo

The similarity of the loss-of-function phenotypes of N-cadherin and Robo2 suggest that they might have parallel or cooperative functions in mediating proper coalescence of placode-derived neurons. To test if they act in concert, we investigated whether altering levels of Slit1-Robo2 signaling affects the expression of N-cadherin in vivo. Control GFP (cytoplasmic or membrane GFP) or dominant-negative (dn) Robo2 (Robo2Δ-GFP) was electroporated into the placodal ectoderm prior to placodal ingression. The distribution of N-cadherin protein on GFP$^+$/TuJ1$^+$ placode-derived neurons was analyzed in serial sections through the placodal ectoderm at stages 13-14, as the first large wave of cells are ingressing in stage-matched control (n=2) and experimental (n=2) embryos.

High-resolution analysis revealed that, under control conditions, N-cadherin was highly concentrated at sites of contact between placodal cells at their intercellular boundaries, as visualized by abundant expression in small groups of placodal cells (Fig. 4A; see Fig. S3 in the supplementary material). That these contact sites represent adherens junctions was confirmed by staining for the adherens junction marker β-catenin (see Fig. S3 in the supplementary material). The distribution of N-cadherin protein appeared dynamic, with high levels at adherens junctions between adherent placode cells, but more punctate expression at the cell membranes of individual cells (Fig. 4A; see Fig. S3 in the supplementary material). Thus, N-cadherin expression levels are non-uniform and appear to depend upon the degree of cell association.

In dnRobo2-treated embryos, placodal neurons failed to form tight adherens junctions and there were reduced levels of N-cadherin at placode cell boundaries (Fig. 4B). Instead, ingressed dnRobo2 placodal neurons appeared more scattered (Fig. 4B). Later, at stage 17, the same trend was observed such that reduction of Robo2 function caused aberrant dispersal of individual placodal neurons concomitant with a reduction in N-cadherin expression at the sites of cell contact (data not shown). These results support the intriguing possibility that Robo2 might regulate the accumulation of N-cadherin in the tight adherens junctions between placodal neurons that are required for their adhesion.

To perform the reciprocal experiments of increasing Slit-Robo expression, we designed a construct encoding the N-terminal portion of chick Slit1 that encompasses the four leucine-rich repeats (cytopcig-Slit1-LRR), shown to be sufficient for binding and activating Robo (Battye et al., 2001; Chen et al., 2001; Howitt et al., 2004; Morlot et al., 2007) and more potent than full-length Slit in rescuing midline axon defects in fly *slit* mutants (Battye et al., 2001). Cytopcig-Slit1-LRR was electroporated into the placodal tissue prior to ingression and ganglia with high levels of transfection in at least one lobe were scored (Fig. 5). 'Mild' effects refer to misshapen ganglia with aggregation defects in regions of the ganglia, whereas 'severe' defects reflect dramatic changes in condensation, including

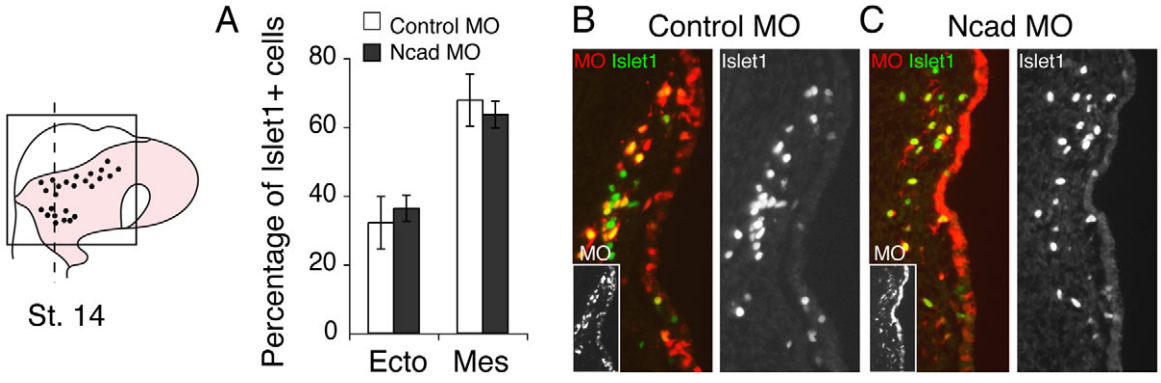

Fig. 3. Morpholino-mediated knockdown of N-cadherin does not block placodal ingression. To the left is a schematic of a stage 14 chick embryo showing the region of analysis (boxed) and the level of sections in B and C (dashed line). (**A**) Bar chart showing that the percentages of Islet1$^+$ placodal cells associated with ectoderm and in the mesenchyme were not significantly different between control MO (n=4) and Ncad MO (n=3) embryos (P=0.43, two-tailed Student's t-test). Error bars, s.d. (**B**,**C**) Left, overlay showing MO transfection (red and inset) and Islet1 (green). Right, single-channel image of Islet1. Compared with control MO embryos (B), placodal cells in the Ncad MO embryos (C) appear more scattered early on at stage 14. Ecto, ectoderm; Mes, mesenchyme.

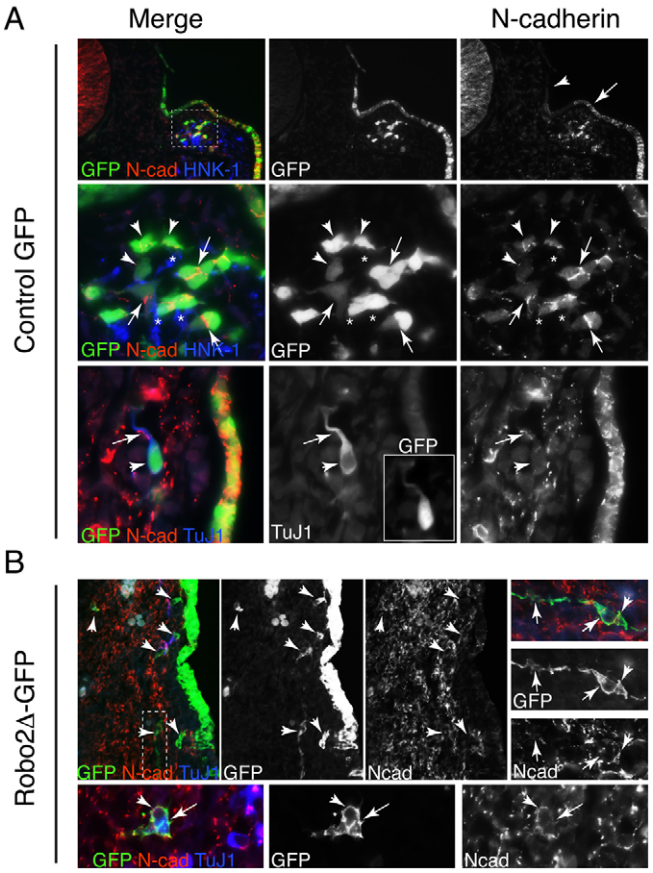

Fig. 4. Robo2 inhibition blocks formation of N-cadherin-localized tight adherens junctions. (**A**) (Top row) Cross-section through a stage 13 control GFP chick embryo showing N-cadherin protein expression in the dorsomedial and ventral ectoderm (arrow) where placodal neurons arise, and not in the most dorsal ectoderm (arrowhead). (Middle row) Higher magnification of the boxed region showing N-cadherin localized at sites of placodal cell-cell contacts (GFP$^+$, arrows) and punctate expression on individual placodal neurons (GFP$^+$, arrowheads). HNK-1$^+$ neural crest cells (blue, stars) associate closely with placodal cells. (Bottom row) N-cadherin is largely downregulated on the cell body of individual placodal neurons (GFP$^+$/TuJ1$^+$), although weak punctate spots remain (arrowhead), and there is prominent expression at the contact site between the neuronal process and another cell (arrow). (**B**) (Top row) Robo2-blocked placodal neurons (GFP$^+$/TuJ1$^+$) are more dissociated and do not have high N-cadherin expression at the cell boundaries (arrowheads). The boxed region is shown (rotated 90 degrees) at higher magnification to the right, showing ingressed Robo2Δ-GFP placodal cells expressing little or no N-cadherin (arrows) and punctate N-cadherin at the cell junction (arrowhead). (Bottom row) Two associating placodal cells blocked by Robo2Δ-GFP do not form N-cadherin-localized adherens junctions (arrow) but still express some N-cadherin on the peripheral cell surface (arrowhead).

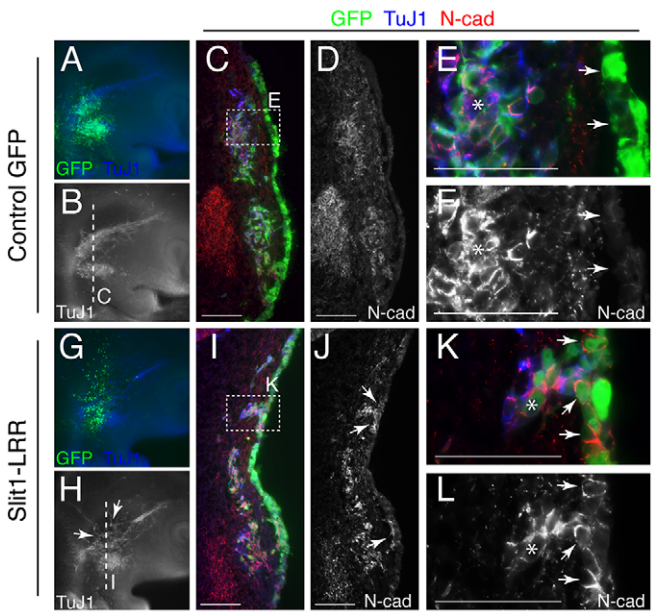

Fig. 5. Ectopic Slit1 expression in the placodal ectoderm leads to increased N-cadherin expression at sites of aberrant placodal clusters. (**A**,**B**) Control GFP chick embryo showing the trigeminal placodal ganglion (GFP$^+$/TuJ1$^+$). (**C**) Frontal plane section through the two trigeminal lobes as indicated in B. (**D**) N-cadherin protein expression in the same section as in C. (**E**,**F**) Higher magnification of boxed region in C showing downregulation of N-cadherin in the surface ectoderm (arrows) but strong expression in the ingressed placodal cells (asterisk). (**G**,**H**) Slit1-LRR-transfected ganglion showing aberrant aggregation of placodal cells (arrows, GFP$^+$/TuJ1$^+$). (**I**,**J**) Frontal plane section as indicated in H. (**K**,**L**) Higher magnification of boxed region in I; N-cadherin is abnormally upregulated in the surface ectoderm (arrows); N-cadherin is also highly expressed in the ingressed placodal cluster (asterisk). Scale bars: 100 μm in C,D,I,J; 50 μm in E,F,K,L.

ectopic aggregates and/or axonal disorganization in at least one lobe. Ectopic expression of Slit1 in the placodal ectoderm caused severe (44% at stages 15-16, n=9; 46% at stages 17-18, n=13) or mild (44% at stages 15-16, n=9; 31% at stages 17-18, n=13) effects in the vast majority of cases. Control GFP embryos at these stages showed no phenotypes (n=18). Furthermore, in severely affected ganglia, N-cadherin expression was upregulated on the cell surface in discrete regions of the ectoderm corresponding to locations near aberrant placodal clusters (Fig. 5K,L) at times when N-cadherin is normally downregulated in the ectoderm at stage 16 (Fig. 5E,F). This defect was more severe in the forming ophthalmic (OpV) than maxillomandibular (MmV) lobe, consistent with our previous finding with Robo2 inhibition (Shiau et al., 2008).

Similarly, overexpression of full-length Robo2 (FL-Robo2) (Reeber et al., 2008) in the placodal ectoderm upregulated N-cadherin at sites of aberrant coalescence (41%, n=17) (Fig. 6B,E,G-N). The FL-Robo2 vector was co-injected with the membrane GFP plasmid to visualize transfected cells by GFP and its Robo2 protein expression was confirmed by myc staining (Fig. 6O-R). In addition, we overexpressed full-length N-cadherin in placodal ectoderm to investigate whether high levels of N-cadherin alone can cause aberrant clustering of placode-derived neurons. This resulted in aberrant aggregates (67%, n=9), similar to those seen after increasing Slit-Robo signaling, although it also caused an apparent loss of placodal neurons (Fig. 6C,F). By contrast, control GFP embryos (n=9) showed no aberrant coalescence (Fig. 6A,D). The upregulation of N-cadherin expression in sites of placodal aggregation during normal development, together with the induced placodal aggregation upon increasing N-cadherin expression by increasing Slit1, Robo2 or N-cadherin, strongly support the idea that Slit-Robo signaling can upregulate N-cadherin on the placodal cell surface, which in turn promotes placodal adhesion.

To test whether the modulation of N-cadherin expression by Slit-Robo occurs at the transcriptional or translational level, we dissected the head regions of stage 13-14 control and Robo2 knockdown

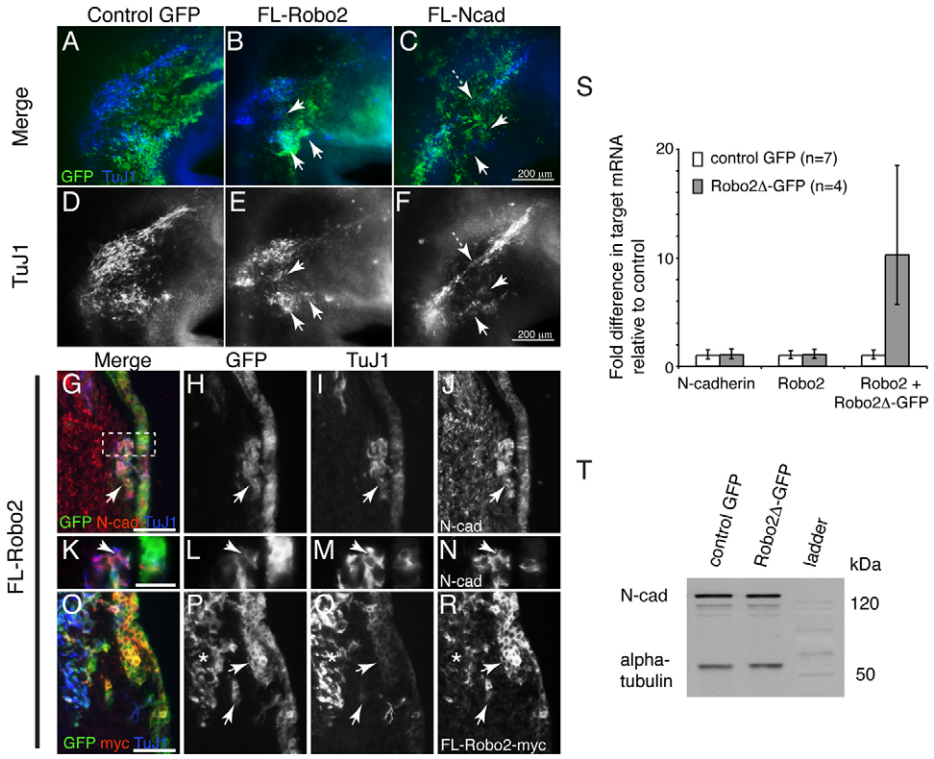

Fig. 6. Overexpression of either Robo2 or N-cadherin leads to abnormal aggregation and increased N-cadherin at contact sites, but total N-cadherin mRNA and protein levels are not altered by blocking Robo2. (**A-F**) Control GFP (A,D), full-length Robo2 (FL-Robo2) (B,E), and full-length N-cadherin (FL-Ncad) (C,F) chick embryos at stage 16. Overexpression of Robo2 (B,E) or N-cadherin (C,F) causes abnormal aggregation in the ganglionic anlage (arrows). N-cadherin overexpression also causes an apparent loss of placodal neurons (dashed arrow). (**G-J**) Sections through the FL-Robo2 embryo showing high N-cadherin expression (arrow) on aberrant placodal aggregates (TuJ1^{+}/GFP^{+}) near the ectoderm. (**K-N**) Higher magnification of the boxed area in G, showing high N-cadherin expression at placodal cell junctions (arrowhead). (**O-R**) Ectopic aggregates near the ectoderm and in the mesenchyme (arrows) express the FL-Robo2-myc protein near the coalescing ganglion (star). (**S**) There is no statistical difference in N-cadherin or endogenous *Robo2* transcript levels between control (*n*=7) and Robo2-inhibited (*n*=4) embryos as assessed by qPCR. As a positive control, a significant (~10-fold on average) increase in the exogenous Robo2Δ-GFP transcript level was detected relative to the control. Error bars, s.d. For supporting details, see Fig. S4 in the supplementary material. (**T**) A representative western blot showing no detectable difference in the total N-cadherin protein level between Robo2Δ-GFP- and GFP-transfected stage 17 head tissues that encompass the trigeminal ganglia. Per lane, 12.5 μg sample was loaded, with α-tubulin as loading control. Scale bars: 50 μm in G-J,O-R; 20 μm in K-N.

embryos in the region containing the forming trigeminal ganglia. cDNA was processed for qPCR analysis with N-cadherin-specific primers (see Fig. S4 in the supplementary material) to measure mRNA levels against an endogenous control (*Gapdh*). We found no significant difference in N-cadherin or endogenous *Robo2* transcript levels between control (*n*=7) and dnRobo2 (*n*=4) embryos (Fig. 6S). Similarly, immunoblots with N-cadherin antibody (*n*=3) showed no significant difference in N-cadherin protein levels between stage-matched control and dnRobo2 head regions (Fig. 6T). Together with the dynamic distribution pattern of N-cadherin protein that appears dependent on the aggregation state of placodal cells, this observation suggests that a post-translational, rather than a transcriptional or translational, change accompanies Slit-Robo signaling. This might involve localization or stabilization of N-cadherin on the placodal cell membrane.

Modulating N-cadherin levels reverses the effects of Slit1-Robo2 perturbations

The observation that the N-cadherin loss-of-function phenotype resembles that of Robo2 inhibition, together with the changes to N-cadherin protein localization on the placodal cell surface upon perturbation of Slit-Robo, suggest a possible synergistic relationship. To examine this possibility further, we tested whether N-cadherin can rescue the effects of Robo2 inhibition in the placodal cells. We co-electroporated full-length N-cadherin (cytopcig + FL-Ncad) or an empty vector control (cytopcig) plus Robo2Δ-GFP into the placodal ectoderm. The results showed that N-cadherin rescues the severely dispersed ganglion phenotype of Robo2 inhibition at stages 15-18 by 31% and overall (mild plus severe) defects by ~40% (*n*=16) as compared with controls (*n*=8) (Fig. 7A,B). The rescued ganglia were markedly less dispersed and more coalesced than those electroporated with Robo2Δ-GFP.

Next, we examined whether depletion of N-cadherin could abrogate the effects of Slit1 overexpression by co-electroporating Slit1-LRR with Ncad MO or control MO into the placodal tissue. In contrast to the severely aberrant ganglia with control MO (*n*=10), reduction of N-cadherin by Ncad MO in Slit1-LRR embryos (*n*=20) significantly decreased the aggregation defects by ~35% overall, and gave rise to normally condensing ganglia (Fig. 7C,D). We note that co-electroporation of either control or Ncad MO with Slit1-LRR plasmid DNA tended to lower the transfection efficiency of the DNA construct. Thus, modulating N-cadherin expression levels significantly reverses the defects of

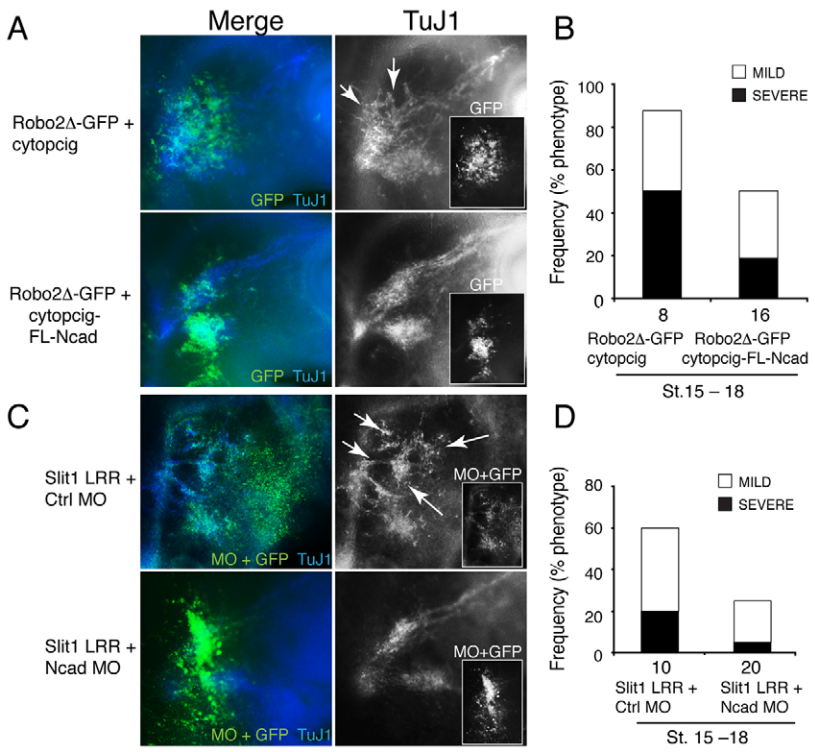

Fig. 7. Modulating N-cadherin expression reverses the effects of Robo2 inhibition and Slit1 overexpression. (**A**) (Top) Co-electroporation of Robo2Δ-GFP and empty vector (cytopcig) leads to severely disorganized and dispersed ganglia (arrows). (Bottom) Co-expression of Robo2Δ-GFP with full-length N-cadherin (cytopcig-FL-Ncad) suppresses the severe effects of blocking Robo2 function, giving rise to normally coalesced ganglia. Grayscale images show single channel of the placodal neuronal marker TuJ1 and of the transfection reporter GFP in the inset. (**B**) Co-expression of FL-Ncad and Robo2Δ-GFP significantly reduces the severe effects of Robo2Δ-GFP by 31% and overall by ~40%. Embryos scored as 'mild' have misshapen ganglia with aggregation defects in regions of the ganglia; those scored as 'severe' have widespread dispersed neurons and markedly abnormal ganglia in at least one lobe. (**C**) (Top) Co-electroporation of Slit1-LRR and control MO in the trigeminal placodal ectoderm leads to severely abnormal patterns of ganglion aggregation (arrows). (Bottom) Co-expression of Slit1-LRR with Ncad MO significantly decreases ganglion coalescence defects. Green, MO tagged with 3′ fluorescein and GFP; blue, TuJ1. (**D**) Co-expression of Slit1-LRR and Ncad MO significantly reduces the effects of Slit1 overexpression, overall by ~35%. Embryos scored as 'mild' have misshapen ganglia with aggregation defects; those scored as 'severe' have dramatic defects in condensation, including ectopic aggregates and/or axonal disorganization in at least one lobe. The number ganglia analyzed (*n*) is shown beneath each bar.

Slit1-Robo2 perturbations, consistent with the possibility that Robo2 and N-cadherin collaborate to mediate proper placodal aggregation into trigeminal ganglia.

Robo2 and Slit1 expression is common to trigeminal and epibranchial regions

Since Slit1-Robo2 interactions have been implicated in assembly of the trigeminal ganglion (Shiau et al., 2008), we asked whether this receptor-ligand pair generally function in neural crest-placode assembly of all cranial sensory ganglia. We further characterized the expression patterns of *Robo2* and *Slit1* in the hindbrain regions of the chick embryo during epibranchial gangliogenesis at stages 16-18. The results showed that the complementary expression pattern of *Robo2* in the placodes and of its ligand *Slit1* in the neural crest is common to all forming epibranchial ganglia (geniculate, petrosal and nodose, which correspond to the facial, glossopharyngeal and vagal cranial nerves, respectively). Transverse sections revealed that *Robo2*-expressing cells in the ectodermal and ingressing placodes intermingle with HNK-1^{+} migratory neural crest cells that co-express Slit1 at stage 16 in the forming facial and glossopharyngeal ganglia (see Fig. S5 in the supplementary material). Similarly, N-cadherin was present on the placodal neurons of all cranial ganglia. This raises the intriguing possibility that Slit1-Robo2 signaling linked to N-cadherin might be a general mechanism for neural crest-placode interaction during chick cranial gangliogenesis.

DISCUSSION

Our results suggest a novel mechanism for chick cranial gangliogenesis whereby Slit1-Robo2 signaling between neural crest and placodal cells regulates adhesion of placodal neurons via modulation and redistribution of N-cadherin protein at the cell surface. Recent in vitro studies (Rhee et al., 2007; Rhee et al., 2002) show that Slit activation of Robo causes phosphorylation of β-catenin by Robo-bound Abelson (Abl) tyrosine kinase, thus inhibiting the link of N-cadherin to the actin cytoskeleton. In vivo studies in *Drosophila* demonstrate that Slit-Robo signaling inhibits E-cadherin to allow cell shape changes for lumen formation in the developing heart tube (Santiago-Martinez et al., 2008). Contrasting with this negative regulation of cadherins, our data in vertebrates suggest that Slit-Robo signaling can also positively regulate cadherin-mediated cell adhesion during chick cranial gangliogenesis. Since this receptor-ligand pair can mediate both repulsive and attractive functions in cell migration and axon patterning (Chedotal, 2007), it is not surprising that Slit-Robo can both positively and negatively regulate cadherin-mediated adhesion, in a context-dependent manner. This might depend on the target tissue, the presence or absence of interacting molecules, and the levels of Slit signaling.

The dynamic expression pattern of N-cadherin in various developing tissues (nervous system, connective tissues, somite, limb, lung, kidney and heart) undergoing morphogenesis suggests a potentially general role for this cell adhesion molecule in cellular condensation and/or organ formation (Duband et al., 1987; El Sayegh et al., 2007; Hatta et al., 1987). N-cadherin has been found to promote coalescence in the forming heart, somite and limb mesenchyme (Linask et al., 1998; Oberlender and Tuan, 1994; Radice et al., 1997). Accordingly, we find that N-cadherin function is essential for the condensation of placodal neurons into cranial ganglia.

Our data suggest that Slit1-Robo2 influences the subcellular localization of N-cadherin protein in placodal neurons. However, there are likely to be other regulators of N-cadherin as its expression is broader than that of Robo2 in the placodal ectoderm. Consistent with this, blocking Slit-Robo signaling by Robo2Δ-GFP does not eliminate N-cadherin expression in the placodal cells, but rather alters its distribution with some apparent diminuition. Conversely, increasing Slit1 or Robo2 expression in the placodal ectoderm

increases expression of N-cadherin protein on the cell surface of placodal cells in aberrant clusters, similar to N-cadherin overexpression. Interestingly, the more severe defects in placodal ingression and axonal projections observed in Robo2-deficient embryos cannot be completely explained by N-cadherin loss-of-function, which affects ganglion condensation but, seemingly, has less of an effect on ingression or axonal pathfinding. Thus, other, yet to be identified effector molecules might mediate Slit1-Robo2 signaling in conjunction with N-cadherin, and N-cadherin is likely to also have independent functions in the placodal ectoderm. Nonetheless, there are many links between N-cadherin and Slit1-Robo2 signaling, including: (1) the similarity of the ganglionic loss-of-function phenotype of N-cadherin and Robo2; (2) the common expression of N-cadherin and Robo2 on assembling placode-derived neurons; (3) the rescue of Robo2 inhibition by full-length N-cadherin; and (4) the changes in N-cadherin protein distribution caused by altering Slit1-Robo2 signaling. Together, these data provide strong evidence for modulation of N-cadherin by Robo2-dependent signaling in placodal neuron aggregation.

How does Slit1-Robo2 regulate N-cadherin expression and/or function in the placodal cells? Our results support the possibility that there is a post-translational change and likely redistribution of N-cadherin that accompanies Slit-Robo signaling, rather than any regulation via transcription or translation of N-cadherin. This might be mediated by convergence of common or interacting intracellular molecules involved with both Robo2 and N-cadherin functions, such as the small Rho GTPases (Rho, Rac, Cdc42) that regulate the actin cytoskeleton. Cadherins can act not only as cell adhesion proteins, but also as signaling molecules that can elicit changes in response to intracellular signals (Yap and Kovacs, 2003). Both Robo (Chedotal, 2007; Ghose and Van Vactor, 2002; Guan and Rao, 2003) and cadherin (Charrasse et al., 2002; Noren et al., 2001; Yap and Kovacs, 2003) signaling have been shown to regulate Rho GTPases, which, conversely, can feedback on cadherin (Braga, 1999; Fukata and Kaibuchi, 2001). Thus, regulation of Rho GTPases might be a point of cross-talk between Robo and cadherin signaling. Independently, Robo2 might regulate other intracellular associations of N-cadherin such as phosphorylation of catenins to regulate cadherin trafficking to the cell surface. Consistent with this possibility, p120 catenin has been shown to stabilize cadherins and regulate their turnover at the cell membrane (Kowalczyk and Reynolds, 2004; Perez-Moreno and Fuchs, 2006). Regulation of cadherin protein on the cell surface is dynamic and may involve various signaling pathways that mediate different routes of endocytosis and internalization (reviewed by Delva and Kowalczyk, 2009).

The common expression of Robo2 and N-cadherin in the trigeminal and epibranchial placodes and Slit1 in all migratory cranial neural crest streams underscores the likelihood of a general mechanism in mediating neural crest-placode interactions in all cranial ganglia. Epibranchial ganglia have a long tubular-like morphology distinct from the bilobed shape of the trigeminal ganglion. However, at times of early cell assembly, the two regions share many features. The distributions of neural crest- and placode-derived cells in the trigeminal and epibranchial ganglia are similar: neural crest cells intermix with placodal neurons and the most proximal regions of the ganglia are solely neural crest derived (Begbie and Graham, 2001; Shiau et al., 2008). Neural crest ablations in both regions cause aberrant projection patterns of placode-derived neurons (Begbie and Graham, 2001; Shiau et al., 2008). In addition, Slit1 is expressed by neural crest cells in both epibranchial and trigeminal regions within discrete time windows during ganglion assembly (Shiau et al., 2008).

The differential expression and function of N-cadherin in placodal, but not cranial neural crest, cells probably relate to their state of neuronal differentiation. Since cranial neural crest cells differentiate into neurons much later in development than placode cells (D'Amico-Martel, 1982; D'Amico-Martel and Noden, 1980), well after the cranial ganglia have formed, they might not begin to express N-cadherin until after gangliogenesis. In support of this, at trunk levels, which lack placodal cells, N-cadherin is expressed in all neural crest-derived peripheral ganglia, both dorsal root and sympathetic (Akitaya and Bronner-Fraser, 1992; Kasemeier-Kulesa et al., 2006). Furthermore, migrating trunk neural crest cells do not express N-cadherin until after they have begun to coalesce and differentiate into neurons (Akitaya and Bronner-Fraser, 1992).

In summary, the present results show that N-cadherin plays a crucial role in driving aggregation of placodal neurons and that it acts together with Slit1-Robo2 interactions in mediating proper trigeminal gangliogenesis. This represents the first in vivo evidence of a functional link between cadherin and Slit-Robo signaling in vertebrate development. Our study also reveals for the first time the formation of adherens junctions containing N-cadherin at sites of placode-placode cell contacts during ganglion assembly in vivo. The similar expression patterns of these molecules in all cranial ganglia suggest a possible unifying mechanism whereby Slit-Robo signaling controls morphogenesis associated with cadherin function in forming the cranial sensory ganglia in the chick embryo. These results demonstrate the importance of heterotypic cell interactions during cranial gangliogenesis for cellular condensation, casting light on the crucial interplay of cell-cell communication and cell adhesion.

Acknowledgements

We thank Drs J. Raper and Z. Kaprielian for the CMV-Robo2FL-myc plasmid; Dr M. Takeichi for the pCMV-cN/FLAG-pA plasmid; members of M.B.-F. laboratory for discussions and technical support; and Dr M. Barembaum for critical comments on the manuscript. This work was supported by US National Institutes of Health (NIH) National Research Service Award 5T32 GM07616 to C.E.S. and NIH grant DE16459 to M.B.-F. Deposited in PMC for release after 12 months.

Supplementary material

Supplementary material for this article is available at
http://dev.biologists.org/cgi/content/full/136/24/4155/DC1

References

Akitaya, T. and Bronner-Fraser, M. (1992). Expression of cell adhesion molecules during initiation and cessation of neural crest cell migration. *Dev. Dyn.* **194**, 12-20.

Baker, C. V. (2005). Neural crest and cranial ectodermal placodes. In *Developmental Neurobiology* (ed. M. S. R. a. M. Jacobson), pp. 67-127. New York: Kluwer Academic/Plenum Publishers.

Battye, R., Stevens, A., Perry, R. L. and Jacobs, J. R. (2001). Repellent signaling by Slit requires the leucine-rich repeats. *J. Neurosci.* **21**, 4290-4298.

Begbie, J. and Graham, A. (2001). Integration between the epibranchial placodes and the hindbrain. *Science* **294**, 595-598.

Braga, V. M. (1999). Small GTPases and regulation of cadherin dependent cell-cell adhesion. *Mol. Pathol.* **52**, 197-202.

Brose, K. and Tessier-Lavigne, M. (2000). Slit proteins: key regulators of axon guidance, axonal branching, and cell migration. *Curr. Opin. Neurobiol.* **10**, 95-102.

Charrasse, S., Meriane, M., Comunale, F., Blangy, A. and Gauthier-Rouviere, C. (2002). N-cadherin-dependent cell-cell contact regulates Rho GTPases and beta-catenin localization in mouse C2C12 myoblasts. *J. Cell Biol.* **158**, 953-965.

Chedotal, A. (2007). Slits and their receptors. In *Axon Growth and Guidance*, vol. 621 (ed. D. Bagnard), pp. 65-80. New York: Landes Bioscience, Springer.

Chen, J. H., Wen, L., Dupuis, S., Wu, J. Y. and Rao, Y. (2001). The N-terminal leucine-rich regions in Slit are sufficient to repel olfactory bulb axons and subventricular zone neurons. *J. Neurosci.* **21**, 1548-1556.

D'Amico-Martel, A. (1982). Temporal patterns of neurogenesis in avian cranial sensory and autonomic ganglia. *Am. J. Anat.* **163**, 351-372.

D'Amico-Martel, A. and Noden, D. M. (1980). An autoradiographic analysis of the development of the chick trigeminal ganglion. *J. Embryol. Exp. Morphol.* **55**, 167-182.
D'Amico-Martel, A. and Noden, D. M. (1983). Contributions of placodal and neural crest cells to avian cranial peripheral ganglia. *Am. J. Anat.* **166**, 445-468.
Delva, E. and Kowalczyk, A. P. (2009). Regulation of cadherin trafficking. *Traffic* **10**, 259-267.
Dickson, B. J. and Gilestro, G. F. (2006). Regulation of commissural axon pathfinding by slit and its Robo receptors. *Annu. Rev. Cell Dev. Biol.* **22**, 651-675.
Duband, J. L., Dufour, S., Hatta, K., Takeichi, M., Edelman, G. M. and Thiery, J. P. (1987). Adhesion molecules during somitogenesis in the avian embryo. *J. Cell Biol.* **104**, 1361-1374.
El Sayegh, T. Y., Kapus, A. and McCulloch, C. A. (2007). Beyond the epithelium: cadherin function in fibrous connective tissues. *FEBS Lett.* **581**, 167-174.
Fukata, M. and Kaibuchi, K. (2001). Rho-family GTPases in cadherin-mediated cell-cell adhesion. *Nat. Rev. Mol. Cell Biol.* **2**, 887-897.
Gammill, L. S. and Bronner-Fraser, M. (2002). Genomic analysis of neural crest induction. *Development* **129**, 5731-5741.
Gammill, L. S., Gonzalez, C. and Bronner-Fraser, M. (2006). Neuropilin 2/semaphorin 3F signaling is essential for cranial neural crest migration and trigeminal ganglion condensation. *J. Neurobiol.* **67**, 47-56.
Ghose, A. and Van Vactor, D. (2002). GAPs in Slit-Robo signaling. *BioEssays* **24**, 401-404.
Guan, K. L. and Rao, Y. (2003). Signalling mechanisms mediating neuronal responses to guidance cues. *Nat. Rev. Neurosci.* **4**, 941-956.
Gumbiner, B. M. (2005). Regulation of cadherin-mediated adhesion in morphogenesis. *Nat. Rev. Mol. Cell Biol.* **6**, 622-634.
Hammond, R., Vivancos, V., Naeem, A., Chilton, J., Mambetisaeva, E., Andrews, W., Sundaresan, V. and Guthrie, S. (2005). Slit-mediated repulsion is a key regulator of motor axon pathfinding in the hindbrain. *Development* **132**, 4483-4495.
Hatta, K. and Takeichi, M. (1986). Expression of N-cadherin adhesion molecules associated with early morphogenetic events in chick development. *Nature* **320**, 447-449.
Hatta, K., Takagi, S., Fujisawa, H. and Takeichi, M. (1987). Spatial and temporal expression pattern of N-cadherin cell adhesion molecules correlated with morphogenetic processes of chicken embryos. *Dev. Biol.* **120**, 215-227.
Howitt, J. A., Clout, N. J. and Hohenester, E. (2004). Binding site for Robo receptors revealed by dissection of the leucine-rich repeat region of Slit. *EMBO J.* **23**, 4406-4412.
Inuzuka, H., Redies, C. and Takeichi, M. (1991). Differential expression of R- and N-cadherin in neural and mesodermal tissues during early chicken development. *Development* **113**, 959-967.
Kasemeier-Kulesa, J. C., Bradley, R., Pasquale, E. B., Lefcort, F. and Kulesa, P. M. (2006). Eph/ephrins and N-cadherin coordinate to control the pattern of sympathetic ganglia. *Development* **133**, 4839-4847.
Kerstetter, A. E., Azodi, E., Marrs, J. A. and Liu, Q. (2004). Cadherin-2 function in the cranial ganglia and lateral line system of developing zebrafish. *Dev. Dyn.* **230**, 137-143.
Kowalczyk, A. P. and Reynolds, A. B. (2004). Protecting your tail: regulation of cadherin degradation by p120-catenin. *Curr. Opin. Cell Biol.* **16**, 522-527.
Linask, K. K., Ludwig, C., Han, M. D., Liu, X., Radice, G. L. and Knudsen, K. A. (1998). N-cadherin/catenin-mediated morphoregulation of somite formation. *Dev. Biol.* **202**, 85-102.
Liu, Q., Ensign, R. D. and Azodi, E. (2003). Cadherin-1, -2 and -4 expression in the cranial ganglia and lateral line system of developing zebrafish. *Gene Expr. Patterns* **3**, 653-658.
MacMullin, A. and Jacobs, J. R. (2006). Slit coordinates cardiac morphogenesis in Drosophila. *Dev. Biol.* **293**, 154-164.
McLarren, K. W., Litsiou, A. and Streit, A. (2003). DLX5 positions the neural crest and preplacode region at the border of the neural plate. *Dev. Biol.* **259**, 34-47.
Morlot, C., Thielens, N. M., Ravelli, R. B., Hemrika, W., Romijn, R. A., Gros, P., Cusack, S. and McCarthy, A. A. (2007). Structural insights into the Slit-Robo complex. *Proc. Natl. Acad. Sci. USA* **104**, 14923-14928.
Nakagawa, S. and Takeichi, M. (1998). Neural crest emigration from the neural tube depends on regulated cadherin expression. *Development* **125**, 2963-2971.
Noden, D. M. (1993). Spatial integration among cells forming the cranial peripheral nervous system. *J. Neurobiol.* **24**, 248-261.
Noren, N. K., Niessen, C. M., Gumbiner, B. M. and Burridge, K. (2001). Cadherin engagement regulates Rho family GTPases. *J. Biol. Chem.* **276**, 33305-33308.
Oberlender, S. A. and Tuan, R. S. (1994). Expression and functional involvement of N-cadherin in embryonic limb chondrogenesis. *Development* **120**, 177-187.
Packer, A. I., Elwell, V. A., Parnass, J. D., Knudsen, K. A. and Wolgemuth, D. J. (1997). N-cadherin protein distribution in normal embryos and in embryos carrying mutations in the homeobox gene Hoxa-4. *Int. J. Dev. Biol.* **41**, 459-468.
Perez-Moreno, M. and Fuchs, E. (2006). Catenins: keeping cells from getting their signals crossed. *Dev. Cell* **11**, 601-612.
Qian, L., Liu, J. and Bodmer, R. (2005). Slit and Robo control cardiac cell polarity and morphogenesis. *Curr. Biol.* **15**, 2271-2278.
Radice, G. L., Rayburn, H., Matsunami, H., Knudsen, K. A., Takeichi, M. and Hynes, R. O. (1997). Developmental defects in mouse embryos lacking N-cadherin. *Dev. Biol.* **181**, 64-78.
Redies, C., Inuzuka, H. and Takeichi, M. (1992). Restricted expression of N- and R-cadherin on neurites of the developing chicken CNS. *J. Neurosci.* **12**, 3525-3534.
Reeber, S. L., Sakai, N., Nakada, Y., Dumas, J., Dobrenis, K., Johnson, J. E. and Kaprielian, Z. (2008). Manipulating Robo expression in vivo perturbs commissural axon pathfinding in the chick spinal cord. *J. Neurosci.* **28**, 8698-8708.
Rhee, J., Mahfooz, N. S., Arregui, C., Lilien, J., Balsamo, J. and VanBerkum, M. F. (2002). Activation of the repulsive receptor Roundabout inhibits N-cadherin-mediated cell adhesion. *Nat. Cell Biol.* **4**, 798-805.
Rhee, J., Buchan, T., Zukerberg, L., Lilien, J. and Balsamo, J. (2007). Cables links Robo-bound Abl kinase to N-cadherin-bound beta-catenin to mediate Slit-induced modulation of adhesion and transcription. *Nat. Cell Biol.* **9**, 883-892.
Santiago-Martinez, E., Soplop, N. H. and Kramer, S. G. (2006). Lateral positioning at the dorsal midline: Slit and Roundabout receptors guide Drosophila heart cell migration. *Proc. Natl. Acad. Sci. USA* **103**, 12441-12446.
Santiago-Martinez, E., Soplop, N. H., Patel, R. and Kramer, S. G. (2008). Repulsion by Slit and Roundabout prevents Shotgun/E-cadherin-mediated cell adhesion during Drosophila heart tube lumen formation. *J. Cell Biol.* **182**, 241-248.
Schwarz, Q., Vieira, J. M., Howard, B., Eickholt, B. J. and Ruhrberg, C. (2008). Neuropilin 1 and 2 control cranial gangliogenesis and axon guidance through neural crest cells. *Development* **135**, 1605-1613.
Shiau, C. E., Lwigale, P. Y., Das, R. M., Wilson, S. A. and Bronner-Fraser, M. (2008). Robo2-Slit1 dependent cell-cell interactions mediate assembly of the trigeminal ganglion. *Nat. Neurosci.* **11**, 269-276.
Vargesson, N., Luria, V., Messina, I., Erskine, L. and Laufer, E. (2001). Expression patterns of Slit and Robo family members during vertebrate limb development. *Mech. Dev.* **106**, 175-180.
Yap, A. S. and Kovacs, E. M. (2003). Direct cadherin-activated cell signaling: a view from the plasma membrane. *J. Cell Biol.* **160**, 11-16.